Integrated setup for the fabrication and measurement of magnetoresistive nanoconstrictions in ultrahigh vacuum

Daniel Stickler,[a] Robert Frömter, Wei Li,[b] André Kobs, and Hans Peter Oepen
Institut für Angewandte Physik, Universität Hamburg, Jungiusstr. 11, 20355 Hamburg, Germany

(Received 5 June 2008; accepted 24 August 2008; published online 3 October 2008)

A UHV instrument is presented for *in situ* fabrication of nanostructures and *in situ* investigation of their magnetoresistance. Nanostructures of diverse shape and size are created from thin films utilizing a focused ion beam. The magnetic nanostructures are contacted via a micromanipulator, which makes it possible to address the individual structures. The system is additionally equipped with a scanning electron microscope column, which is used for damage-free navigation and control of the structuring and contacting. First magnetoresistance measurements of structures carved into a Permalloy film demonstrate the high sensitivity and the flexibility of the new setup.
© *2008 American Institute of Physics.* [DOI: 10.1063/1.2981693]

I. INTRODUCTION

In the field of magnetoelectronics and spin-electronics[1–4] one of the main topics is the magnetoresistance (MR) of films and nanostructures,[5–9] in particular, for the application as sensors or read/write devices. Usually, the films are nanostructured by means of UV or e-beam lithography. The latter techniques require various preparation steps under ambient conditions. Such procedures bear problems, in particular, when thin film nanostructures and devices are studied, as their surface to bulk ratio is large and the devices or nanostructures become unstable against oxidation. The focused ion beam (FIB) technique has the potential to overcome the obstacle of multisequential processing and handling of the samples under ambient conditions, as it allows to perform the nanostructuring in high vacuum.[10–14] In many cases of FIB application, however, the samples are transferred under non-ideal conditions into a separate experimental setup for the MR measurements after structuring. The best choice is to perform structuring and measurements within the same UHV system, particularly in case one dimension becomes negligibly small. First UHV experiments on magnetotransport of such nanostructures have been reported recently. In one approach prestructured samples are fine-tuned via conventional nonspatially resolving Ar ion milling and MR investigations are performed in the same vacuum system.[15] In a second approach,[16] the sample is transferred under vacuum from a low energy ion milling stage to the measurement stage. Both methods are good but time consuming when systematic studies require frequent sample exchange. The highest flexibility and efficiency can be achieved if structuring and MR measurements are accomplished in the same position without any sample exchange. Such experiments under UHV have become feasible as only recently FIB systems operating under UHV conditions have become commercially available.

A second class of experiments on ultrathin nanostructures utilizes the magnetotransport as a highly sensitive tool to investigate the magnetic properties of single and/or arrays of nanomagnets.[17–19] In this field as well as in magnetotransport the transition to almost perfect, i.e., single crystalline, monolayer, and epitaxial films[20–22] are rarely found in literature. These topics we want to address in the future with the new instrument.

In this paper we will present our design of a UHV system that allows to perform nanofabrication and resistance measurements *in situ*, and even simultaneously, in monolayer thick nanostructures. This paper is organized as follows: in the second paragraph we will describe the UHV setup which is mainly a dual beam system, combining a FIB, a scanning electron microscope (SEM), and a stage for MR measurements. Main component of the latter is a micromanipulator controlled probe to electrically contact the nanostructures. The SEM allows to control the structuring and positioning of the probe for resistance measurements, which is explained in detail in the third paragraph. Finally we will show, as proof of principle, some measurements on a film system, which is well known from literature, demonstrating the abilities of our new instrument.

II. EXPERIMENTAL SETUP

A. The UHV FIB/SEM dual beam system

To control the FIB milling and all ion beam manipulation it is most advantageous to include a nondestructive microscope with at least similar lateral resolution. SEM can meet this requirement. For some years so-called dual beam systems, the integration of SEM and FIB into one chamber, are commercially available. The two columns generate two beams, electrons and ions, which have been aligned to hit the sample in the same small area. To achieve best performance for imaging as well as for structuring the sample can be tilted about an axis parallel to the sample surface, which is perpendicular to the mounting plane of SEM and FIB. Thus it is possible to bring the sample in the best position (normal

[a]Electronic mail: daniel.stickler@physnet.uni-hamburg.de.
[b]Present address: University of British Columbia, 2355 East Mall, Vancouver BC, Canada V6T 1Z4.

 © 2008 American Institute of Physics

Downloaded 03 Oct 2008 to 134.100.106.3. Redistribution subject to AIP license or copyright; see http://rsi.aip.org/rsi/copyright.jsp

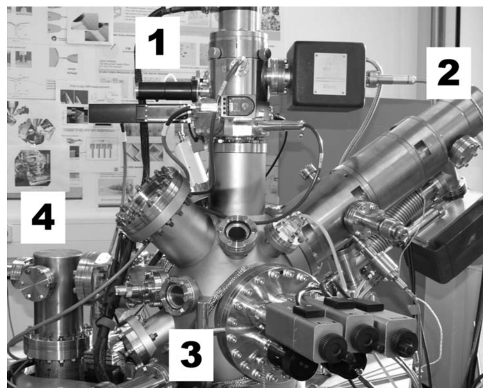

FIG. 1. Side view of the UHV dual beam system with (1) the FIB column in the vertical direction, (2) SEM column arranged at 58°, (3) motorized goniometer stage, and (4) the fast entry lock. The small ports below the FIB column are designated for mounting of an e-beam evaporator. Further ports for evaporators are on the other side.

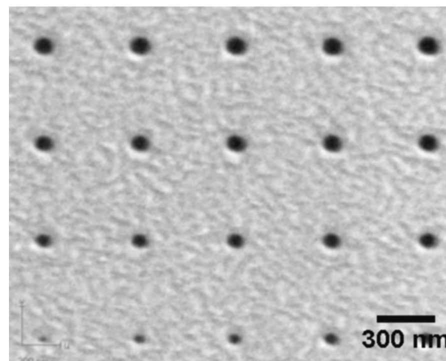

FIG. 3. FIB micrograph of milled pores starting at 0.1 pC in a Pd coated 30 nm thick silicon nitride membrane. The dose has been increased from 0.1 to 2.0 pC, in 0.1 pC steps. A minimum hole size of 20 nm is obtained for 0.1 pC.

incidence) for either FIB or SEM operation. Commercial dual beam systems operate under high vacuum conditions. Following similar design criteria we have built a UHV FIB/SEM instrument with a FIB,[23] a SEM,[24] a goniometer stage,[25] and a transfer system for the fast entry of externally prepared thin film templates.

A side view of the system is shown in Fig. 1. The FIB column (1) is mounted in the vertical position pointing downward, while the SEM column (2) is arranged at 58° to the vertical. Both columns have separate ion pumps attached. The goniometer stage (3, front) is oriented perpendicular to both instruments while the sample transfer (4) axis is in the horizontal plane and passes through the intersection point of the beams. As we were aiming primarily at ultra-fine structuring, special care was taken to achieve optimal performance with FIB application. The FIB column was put in the vertical direction (Fig. 1) to obtain highest stability and to prevent any bending of the instrument due to the long mounting length (specimen to flange distance of 252 mm). For SEM application we accept a slight degradation of performance due to an inclined mounting. In our design the SEM is mainly used for damage-free navigation and observation (Figs. 7 and 8), which does not require ultimate resolution. With FIB imaging a resolution of 10 nm at 1 pA and 30 kV has been achieved. Figure 2 (a) shows a FIB micrograph of graphite flakes and a line scan across the edge of a flake. The line scan of Fig. 2 (b) demonstrates a resolution of 10 nm from a Gaussian fit which equals the stated specification of the ion gun. The resolution of the SEM is about 25 nm at 30 kV and 100 pA.

The chamber body is built from 62 mm thick stainless steel with Conflat flanges to improve stability and to maintain bake out capability. Several ports are designated for mounting of e-beam evaporators for *in situ* epitaxial film growth (see Fig. 1). The main chamber is pumped by an ion pump (400 l/s) and the transfer system is equipped with a turbomolecular pump. The base pressure in the main chamber is in the mid 10^{-10} mbar range. The whole system is supported by an active vibration damping system.

For milling, typical probe currents of 20 pA at 30 kV are used. With these parameters an area of 1 μm^2 in a 30 nm thick Permalloy (Py) film can be fully removed within 10 s. The corresponding milling rate is 0.28 ± 0.08 $\mu m^3/nC$. To achieve the highest flexibility for structuring, a digital pattern generator[26] is used to steer the ion beam. The same hardware is used for image acquisition with FIB. Figure 3 shows the FIB image of a sequence of milled pores with increasing dot dose in a Pd coated 30 nm thick silicon nitride membrane. The smallest pore size of 20 nm is obtained by applying a dose of 0.1 pC.

B. *In situ* MR measurement setup

For the *in situ* investigation of the MR a small electromagnet is incorporated (Fig. 4) and a micromanipulator[27] is

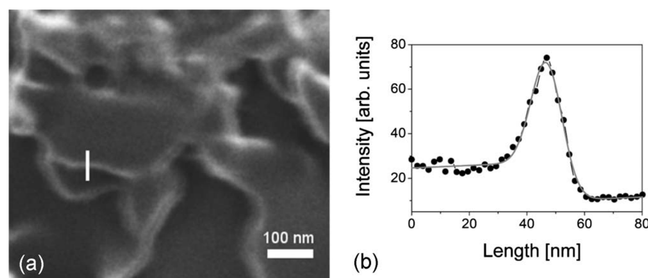

FIG. 2. Scanning ion micrograph of graphite flakes (a). Line scan (b) along the line indicated on the image. The plot is created from the secondary electron detector signal. A resolution of 10 nm is obtained from a Gaussian fit (imaging mode).

FIG. 4. Photograph of the interior of the dual beam system, showing the yoke with coil on the left hand side and the micromanipulator on the right hand side.

Downloaded 03 Oct 2008 to 134.100.106.3. Redistribution subject to AIP license or copyright; see http://rsi.aip.org/rsi/copyright.jsp

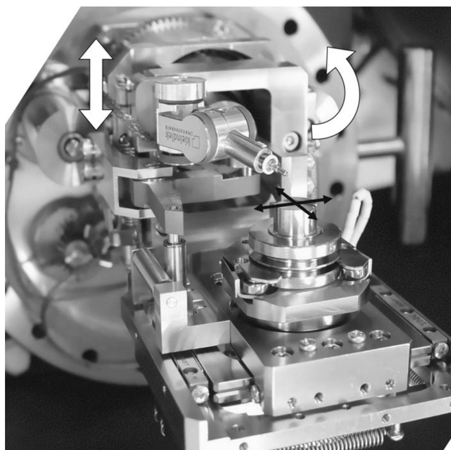

FIG. 5. Five-axis sample stage with the micromanipulator rigidly attached to the main support frame of the stage. The micromanipulator can be moved upward and downward and tilted together with the sample (white arrows), while the sample can be moved in the *xy*-plane (black arrows) and rotated after lifting the tip.

attached to the goniometer stage (Fig. 5).

To the end of the jib of the micromanipulator a very thin tungsten wire (diameter of 25 μm) with a sharp tip is welded, which can be used to form point contacts to any position on the sample. In particular, it allows to electrically connect a FIB fabricated nanostructure. The principle of resistance measurement is sketched in Fig. 6. A metal (ferromagnetic) film is deposited onto an insulating substrate. Via FIB the film is structured to create a nanowire that is connected to the film on one side. The tip of the micromanipulator is used to contact the other side of the nanowire. The resistance of the wire can be measured when a current is applied to the film through the tip. The MR measurements can be done in the presence of a magnetic field. As the FIB offers the possibility to make numerous structures in films of mm^2 dimensions, while the micromanipulator allows their individual addressing, we gain the capability to perform a series of numerous measurements utilizing the same film. This unique combination of *in situ* preparation and investigation saves time, and offers a high flexibility in studying size and shape effects while material parameters remain unchanged.

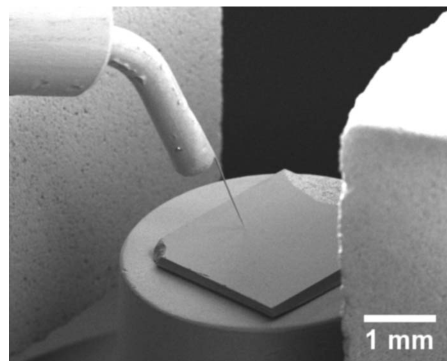

FIG. 7. SEM micrograph (side view) of the sample and the tip in the gap between the pole pieces of the electromagnet.

The micromanipulator is rigidly attached to the frame of the stage (see Fig. 5), which can be tilted and moved in the vertical direction. The horizontal drives of the stage move the sample with respect to the micromanipulator and are used to position the sample under the tip within the crossing point of SEM and FIB beams. Fine positioning of the W tip can be done with submicrometer precision utilizing the electronics of the micromanipulator. The tip approach is monitored via SEM, which, because of its tilt against the sample surface, gives a side view of both surface and tip (Figs. 7 and 8). We do not observe any vibrations of the tip in the SEM when moving the micromanipulator with smallest step mode, so precise positioning is possible. Peng *et al.*[28] reported that they could not resolve any drift in the range of interest (<50 nm) over 1 h for an identical micromanipulator. Although all measurements presented here use a single probe to measure the resistance, this is no hard limitation of the instrument. For cases beyond the demonstrated applicability of the single probe technique, a commercially available four point probe head can be fitted to the micromanipulator.[29] However, due to the much larger extent of such a probe head, larger film areas need to be milled, so some speed and versatility of the method will be lost.

The electromagnet is made of a ferrite yoke wound by copper wire of 0.5 mm diameter. The yoke has a gap of 6 mm. The 250 turns coil has a resistance of less than 0.7 Ω, which is low enough to prevent significant current induced

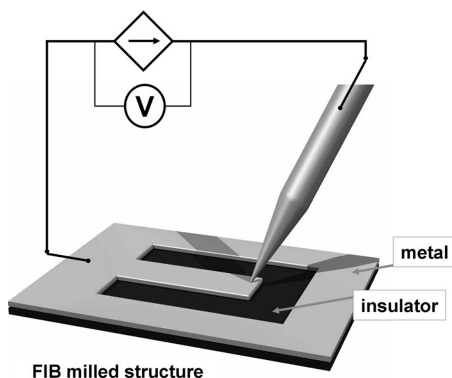

FIG. 6. Schematic of the MR measurement setup: a metal film is deposited onto insulating substrate and a nanowire is created by FIB milling, which remains connected to the grounded film on one side. The resistance can be measured when the tip is navigated to connect the end of the wire.

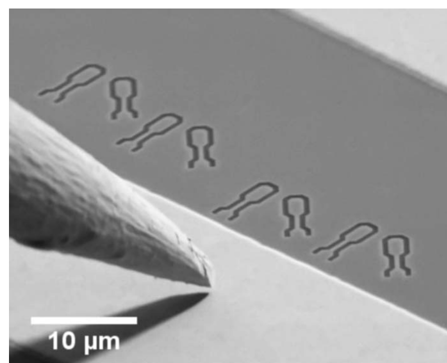

FIG. 8. SEM micrograph of the sample and the W tip. Several test samples, consisting of a wider contact pad and a short section of nanowire, are milled into a 30 nm Permalloy film between two 30 μm wide and 250 nm thick Au stripes (bright regions).

Downloaded 03 Oct 2008 to 134.100.106.3. Redistribution subject to AIP license or copyright; see http://rsi.aip.org/rsi/copyright.jsp

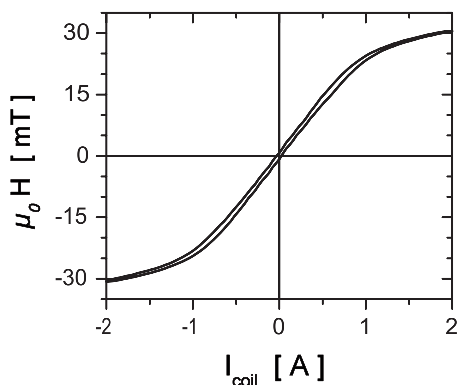

FIG. 9. Flux density ($\mu_0 H$) vs current (I_{coil}) calibration curve of the electromagnet.

heating and minimizes the outgassing of the magnet system and any considerable increase in residual gas pressure during measurements. The electromagnet is mounted via a titanium holder (see Fig. 4) on a linear feedthrough. So the magnet can be retracted to clear the room for sample exchange. In the measuring position the sample is carefully centered between the pole pieces while the tip has full access to every point of the sample. The SEM image of Fig. 7 displays the contacting of the sample via the W tip attached to the micromanipulator. The side planes of the ferrite yoke are large compared to the sample and the nanostructures that are located in the center of the gap. Thus the magnetic field can be considered homogeneous at the position of the nanostructures.

To study the influence of the field direction on the transport properties, the angle between structure and magnetic field has to be varied. FIB nanostructuring allows to perform such studies without any sample manipulation, in the way that the same nanostructure is created multiply at different azimuthal orientations with respect to the magnetic field (as shown in Fig. 8). Although the micromanipulator has to be retracted for the milling of new contact pads, the trim of the structures can be performed even during the MR measurements.

The magnetic field of the electromagnet was calibrated by means of a Hall probe. The flux density, $\mu_0 H$, as a function of the applied current, I_{coil}, is plotted in Fig. 9. The magnetization behavior shows a very small remanence with almost linear field/current dependence up to 19.5 mT/0.8 A. The magnetic field obtained at maximum current (2 A) is 31 mT. The calibration curve is used to determine the field strength from the current values.

III. MEASUREMENT SCHEME

Figure 8 shows typical nanostructures created in a Permalloy film on an insulating substrate (silicon nitride). The dark contours are areas where the film has been removed by FIB milling. Each structure consists of a wider pad (size of about 2 μm^2) for access by the micromanipulator and a narrow wire with dimensions of 4.2×0.5 μm^2, which forms the electrical connection between pad and metal film. The resistance of the wire dominates the overall resistance as well as the MR. The resistance of the film and W needle is very small, but not negligible. This undesired contribution to the galvanomagnetic effect can be eliminated by subtracting the resistance measured with the tip positioned behind (on the pad) and before (on the film) the narrow ultrathin wire. As the magnetization reversal is, in general, a stochastic effect, the subtraction cannot eliminate all the resistance features induced by the film. To overcome this obstacle, 250 nm thick and 30 μm wide Au stripes are grown as shunt on top of the magnetic film via mask techniques before the film is inserted. Close to the Au stripes the nanostructures are fabricated in the noncovered ferromagnetic material. The brighter regions in Fig. 8 are the Au stripes.

Another source of undesired resistance is the contact resistance of the tip to the nanostructure pad. When a very sharp tip is used, the contact area can be very small yielding high resistance. Therefore a rounded tip is produced with FIB (diameter of 300 nm) and a special procedure is carefully followed to ensure a stable Ohmic contact: while the tip approaches the nanostructure the electrical loop is grounded to prevent charging and high discharge currents that could damage the nanowire. The whole process is monitored via SEM. The movement of the tip toward the sample surface is stopped when a slight bending of the tip is recognizable. Then the grounding is removed and resistance measurement is performed. The resistance is usually found to drift over time. The drift is probably caused by further discontinuous sliding of the tip across the pad due to the strain that is created during tip bending. To stop the resistance drift the tip is lifted in the lowest velocity mode until the resistance change vanishes. The reproducibility of the resistance of a structure is better than 3%.

A programmable current source and a nanovoltmeter are used to measure the MR.[30] The current source allows flexible time shaping of the output current. Current pulses of 0.5–12 ms duration can be generated with a maximum repetition rate of 10 Hz. The nanovoltmeter has sampling features that match the timing sequences of the source. The pulse current mode is superior to a dc measurement as higher signal to noise (S/N) ratios can be attained and the average power fed into the device during measurement is reduced. S/N ratios of greater than 10^5 are achievable when synchronization with the frequency of mains is made.

IV. RESULTS AND DISCUSSION

A. Zero-field measurements

The results in the discussion below have been obtained with samples of the following structure: the substrate is a 100 nm thick silicon nitride layer on silicon, on which a 30 nm $Ni_{81}Fe_{19}$ Permalloy (Py) film is grown by thermal deposition, capped by a 3 nm Pt layer to prevent oxidation. Using structures as shown in Fig. 8, we first investigate the temperature versus current behavior and its influence on resistance. The resistance as a function of current for a given pulse period of 100 ms (pulse width of 10 ms) is shown in Fig. 10. The different curves in Fig. 10 represent the resistance versus current dependence for three sequential current sweeps. In the first sweep (solid squares) up to 11 mA, the annealing effects lower the wire resistance as it manifests by

Downloaded 03 Oct 2008 to 134.100.106.3. Redistribution subject to AIP license or copyright; see http://rsi.aip.org/rsi/copyright.jsp

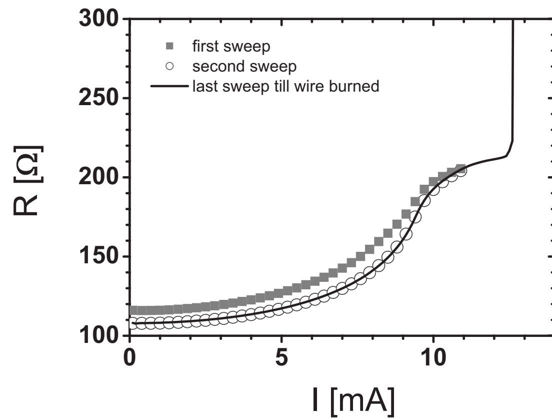

FIG. 10. Resistance vs current plot. The current was pulsed (duration of 10 ms, 10 Hz). The Py wire has a thickness of 30 nm. The characteristics for three successive sweeps are shown (first sweep: solid squares, second/third run: open circles/solid line). The resistance increases due to a current induced temperature rise. From the first to the second run the base resistance at $I \sim 0$ mA is lowered due to annealing effects during the first run. The second sweep covers the same current interval. No further annealing is found while the resistance/current dependence of the third run is absolutely identical to that of the second run. Increasing the current beyond 12 mA (7.6×10^{11} A/m^2) finally destroys the wire.

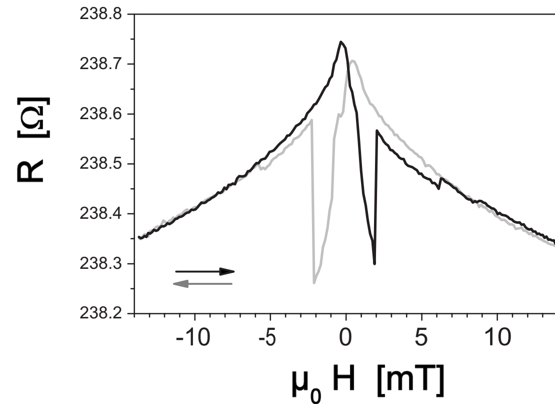

FIG. 12. MR measurement at room temperature. The angle between current and magnetic field direction was 45°. The structure is the same as shown in Fig. 8. A pulsed current with 0.1 mA and 10 ms pulse width with a frequency of 10 Hz was used (the black curve goes from negative to positive magnetic field values).

comparing the first run with the second (open circles) and third (solid line) runs. The resistance/current characteristic in the third run is completely identical to that of the second run, which indicates that the nonlinearity of the curve is no longer caused by a structural change in the wire material. As a temperature/current calibration is not available a further discussion of the curve is rather speculative and will be omitted. On a current increase to 12.6 mA (7.6×10^{11} A/m^2) the wire is destroyed and the resistance goes to infinity. The burned wire with the tip still in measuring position is shown in Fig. 11. The resistance versus current curves demonstrates that in the range from 0.1 to 0.5 mA heating and its effect on resistance can be neglected. Therefore a default current of 0.1 mA has been used in our MR measurements to ensure that temperature effects will not influence the results.

B. MR measurements

The result of a MR measurement at room temperature is shown in Fig. 12. The shape of the structure under investigation is the same as that shown in Fig. 8. The wire dimensions are 5.0×1.5 μm^2 with a thickness of 15 nm. The magnetic field was applied at 45° to the axis of the Py wire within the film plane. The current pulses with a height of 0.1 mA had a duration of 10 ms and a repetition rate of 10 Hz. The overall resistance change in a field sweep up to 14 mT is 0.5 Ω, which is due to the fact that the resistance in a ferromagnet depends on the magnetization orientation with respect to the direction of current flow, the so-called anisotropic MR.[34] A field of 14 mT turns the magnetization out of the direction along the wire axis which is the so-called easy axis of magnetization. As for Py the resistance is smallest when current and magnetization are perpendicular to each other the resistance will drop with increasing angle. Decreasing the field means that the magnetization turns back into the direction along the wire and the resistance will increase. The large jump at 2 mT appears when the field is strong enough to reverse the magnetization along the easy axis of magnetization. In that case a reversed domain is nucleated and rushes through the wire and the magnetization component along the wire axis is switched instantaneously (with respect to the time scale of the measurements).

The scatter of the resistance values is less than 4 mΩ which allows to easily resolve small resistance jumps like that at −6 mT in Fig. 12, which corresponds to a resistance change of R=9.8 mΩ, i.e., the relative change in resistance is $\Delta R/R = 4.1 \times 10^{-5}$.

As explained in the foregoing text one can isolate the effects of the wires from the parasitic effects of the whole system by comparing the MR measured behind the wire (on the pad) and before the wire (on the film). The results of such measurements are shown in Fig. 13 with similar structure and the same field geometry as in the previous example. The size of the wire is 1.2×0.5 μm^2. The plot with an average resistance in the range of 87 Ω (upper curve) represents the measurement with the tip on the pad. The lower resistance value of about 23 Ω on average (lower curve) was measured at the connecting point of the wire to the film. The difference of the averaged resistance values (64 Ω) can be appointed to the resistance of the wire. Both measurements show a resistance change upon field sweep, indicating also MR effects in the film. The resistance change in the whole system is

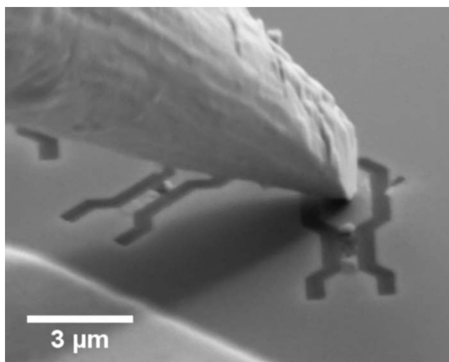

FIG. 11. SEM micrograph of a destroyed wire with the tip still in measuring position.

Downloaded 03 Oct 2008 to 134.100.106.3. Redistribution subject to AIP license or copyright; see http://rsi.aip.org/rsi/copyright.jsp

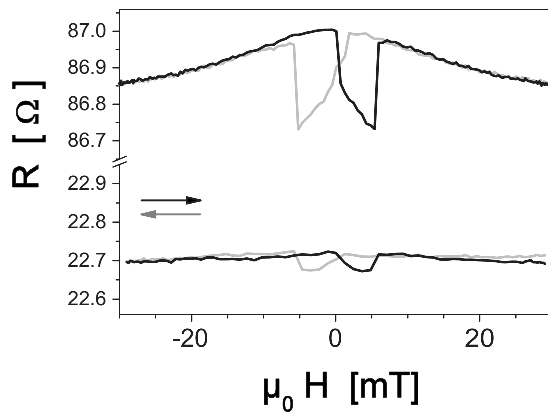

FIG. 13. MR measurements with the tip on the pad (upper curve) and the tip on the film, i.e., before the wire (lower curve). The structure is the same as shown in Fig. 9.

260 mΩ while the change in the film is 44 mΩ. The relative changes are 3×10^{-3} for the wire and 1.94×10^{-3} for the film. The discrepancies of these two measurements might be due to the fact that the magnetic anisotropies of wire and film are different and both have respective easy axes of magnetization. It should be mentioned that the anisotropy of the wire is determined by the shape, which is manipulated on purpose. Both measurements show a resistance jump around 5.4 mT. This indicates that a domain is injected from the film into the wire while the film acts as an injection pad.[31–33] The domain wall is not pinned in front of the constriction, i.e., the narrow wire. If solely the magnetic behavior of the nanostructure is of interest, it will be possible to destroy the magnetism of the film in the transition region by low dose ion milling.

The magnetoresistivity $\Delta\rho=[\rho_0-\rho_{H,\mathrm{sat}}]$ for Py wire measured with the external field perpendicular to the easy axis (the wire axis) is 0.58 ± 0.03 $\mu\Omega$ cm which fits very well into the span of published data for Py.[34,35]

Recently a new topic has appeared in the field of nanomagnetism, i.e., the current induced magnetization switching and domain wall movement. To induce domain wall motion, current densities in the range of 10^{12} A/m^2 are needed.[36] Such current densities can be realized in our setup (see Fig. 10). The current densities that appear in the MR measurements presented here are on purpose far below the critical value at which domain wall movement can be initiated.

V. CONCLUSION

A new instrument for *in situ* fabrication of nanostructures in thin films and *in situ* investigation of their MR is presented. A dual beam system is combined with a micromanipulator based setup for locally measuring the MR. First test measurements demonstrate the high sensitivity and flexibility of the new setup.

ACKNOWLEDGMENTS

The FIB system was funded by the BMBF and Freie und Hansestadt Hamburg via Grant No. HBFG1021-627. We acknowledge the financial support for the micromanipulator by the European Science Foundation via Grant No. NMP4-CT-2003-505282 BMR.

[1] C. Chappert, A. Fert, and F. N. Van Dau, Nat. Mater. **6**, 813 (2007).
[2] H. Coufal, L. Dhar, and C. D. Mee, MRS Bull. **31**, 294 (2006).
[3] C. H. Marrows, Adv. Phys. **54**, 585 (2005).
[4] S. A. Wolf, D. D. Awschalom, R. A. Buhrman, J. M. Daughton, S. von Molnar, M. L. Roukes, A. Y. Chtchelkanova, and D. M. Treger, Science **294**, 1488 (2001).
[5] G. A. Prinz, Science **282**, 1660 (1998).
[6] A. D. Kent, J. Yu, U. R. Rüdiger, and S. S. P. Parkin, J. Phys.: Condens. Matter **13**, R461 (2001).
[7] C. Hassel, M. Brands, F. Y. Lo, A. D. Wieck, and G. Dumpich, Phys. Rev. Lett. **97**, 226805 (2006).
[8] K. I. Bolotin, F. Kuemmeth, A. N. Pasupathy, and D. C. Ralph, Nano Lett. **6**, 123 (2006).
[9] U. Ebels, A. Radulescu, Y. Henry, L. Piraux, and K. Ounadjela, Phys. Rev. Lett. **84**, 983 (2000).
[10] C. A. Volkert and A. M. Minor, MRS Bull. **32**, 389 (2007).
[11] J. Orloff and M. Utlaut, *High Resolution Focused Ion Beams: FIB and its Applications* (Kluwer, Dordrecht, 2002).
[12] J. Orloff, Rev. Sci. Instrum. **64**, 1105 (1993).
[13] L. A. Giannuzzi and F. A. Stevie, *Introduction to Focused Ion Beams: Instrumentation, Theory, Techniques, and Practice* (Springer, Berlin, 2005).
[14] S. Khizroev and D. Litvinov, Nanotechnology **15**, R7 (2004).
[15] D. Morecroft, J. L. Prieto, C. W. Leung, G. Burnell, M. G. Blamire, and D. B. Jardine, J. Appl. Phys. **91**, 8575 (2002).
[16] Y. Ohsawa, J. Magn. Magn. Mater. **287**, 491 (2005).
[17] T. Ono, H. Miyajima, K. Shigeto, K. Mibu, N. Hosoito, and T. Shinjo, Science **284**, 468 (1999).
[18] M. Brands and G. Dumpich, J. Appl. Phys. **98**, 014309 (2005).
[19] M. Kläui, C. A. F. Vaz, J. A. C. Bland, W. Wernsdorfer, G. Faini, E. Cambril, L. J. Heyderman, F. Nolting, and U. Rüdiger, Phys. Rev. Lett. **94**, 106601 (2005).
[20] U. Ruediger, J. Yu, S. Zhang, A. D. Kent, and S. S. P. Parkin, Phys. Rev. Lett. **80**, 5639 (1998).
[21] U. Rüdiger, J. Yu, L. Thomas, S. S. P. Parkin, and A. D. Kent, Phys. Rev. B **59**, 11914 (1999).
[22] C. Hassel, F. M. Römer, R. Meckenstock, G. Dumpich, and J. Linder, Phys. Rev. B **77**, 224439 (2008).
[23] CANION 31 Plus, Orsay Physics, www.orsayphysics.com
[24] Stripped column from a JAMP-30 Auger-Microprobe, JEOL Ltd., www.jeol.com
[25] AP-81030, JEOL Ltd.
[26] ELPHY Quantum, Raith GmbH, www.raith.com.
[27] MM3A-EM UHV, kleindiek nanotechnik, www.nanotechnik.com.
[28] L. M. Peng, Q. Chen, X. L. Liang, S. Gao, J. Y. Wang, S. Kleindiek, and S. W. Tai, Micron **35**, 495 (2004).
[29] S. Hasegawa, N. Sato, I. Shiraki, C. L. Petersen, P. Bøggild, T. M. Hansen, T. Nagao, and F. Grey, Jpn. J. Appl. Phys., Part 1 **39**, 3815 (2000).
[30] Models 6221/2182A Delta Mode system, Keithley Instruments Inc., www.keithley.com.
[31] K. Shigeto, T. Shinjo, and T. Ono, Appl. Phys. Lett. **75**, 2815 (1999).
[32] R. P. Cowburn, D. A. Allwood, G. Xiong, and M. D. Cooke, J. Appl. Phys. **91**, 6949 (2002).
[33] M. Brands and G. Dumpich, J. Phys.: Condens. Matter **38**, 822 (2005).
[34] T. R. McGuire and R. I. Potter, IEEE Trans. Magn. **11**, 1018 (1975).
[35] W. Y. Lee, M. F. Toney, P. Tameerug, E. Allen, and D. Mauri, J. Appl. Phys. **87**, 6992 (2000).
[36] A. Yamaguchi, T. Ono, S. Nasu, K. Miyake, K. Mibu, and T. Shinjo, Phys. Rev. Lett. **92**, 077205 (2004).

Downloaded 03 Oct 2008 to 134.100.106.3. Redistribution subject to AIP license or copyright; see http://rsi.aip.org/rsi/copyright.jsp